Understanding the seasonality, trends and controlling factors of Indian Ocean acidification over distinctive bio-provinces

Kunal Madkaiker[1,2,3], Vinu Valsala[3], M. G. Sreeush[5,6], Anju Mallissery[3], Kunal Chakraborty[4], Aditi Deshpande[2]

[1]Indian Institute of Technology, Delhi, New Delhi, India.

[2]Department of Atmospheric and Space Sciences, Savitribai Phule Pune University, Pune, India

[3]Indian Institute of Tropical Meteorology, Ministry of Earth Sciences, Pune, India

[4]Indian National Centre for Ocean Information Services (INCOIS), Ministry of Earth Sciences, Hyderabad, India

[5]Centre for Climate Physics, Institute for Basic Science (IBS), Busan, Republic of Korea, 46241.

[6]Pusan National University, Busan, Republic of Korea, 46241.

Corresponding author: Kunal Madkaiker (Kunal.Ajit.Madkaiker@cas.iitd.ac.in)

Key Points:

- Controlling factors of the seasonal variability of pH and its trends over various Indian Ocean bio-provinces are investigated.
- DIC and SST are major driving forces contributing to the seasonal variability and trends in pH and counterbalance over the Indian Ocean.
- SST trends directly correlate with acidification trends in IO bio-provinces, indicating that ocean warming enhances acidification.

Abstract

The Indian Ocean (IO) is witnessing acidification as a direct consequence of the continuous rising of atmospheric CO_2 concentration and indirectly due to the rapid ocean warming, which disrupts the pH of the surface waters. This study investigates the pH seasonality and trends over various bio-provinces of the IO and regionally assesses the contribution of each of its controlling factors. Simulations from a global and a regional ocean model coupled with biogeochemical modules were validated with pH measurements over the basin, and used to discern the regional response of pH seasonality (1990-2010) and trend (1961-2010) in response to changes in Sea Surface Temperature (SST), Dissolved Inorganic Carbon (DIC), Total Alkalinity (ALK) and Salinity (S). DIC and SST are significant contributors to the seasonal variability of pH in almost all bio-provinces. Total acidification in the IO basin was 0.0675 units from 1961 to 2010, with 69.3% contribution from DIC followed by 13.8% contribution from SST. For most of the bio-provinces, DIC remains a dominant contributor to changing trends in pH except for the Northern Bay of Bengal and Around India (NBoB-AI) region, wherein the pH trend is dominated by ALK (55.6%) and SST (16.8%). Interdependence of SST and S over ALK is significant in modifying the carbonate chemistry and biogeochemical dynamics of NBoB-AI and a part of tropical, subtropical IO bio-provinces. A strong correlation between SST and pH trends infers an increasing risk of acidification in the bio-provinces with rising SST and points out the need for sustained monitoring of IO pH in such hotspots.

Plain Language Summary

Global oceans are witnessing ocean acidification as a combined result of ocean warming and increased atmospheric CO_2 concentration. Indian Ocean (IO), is a mild sink of CO_2 and its strength is decreasing day by day owing to acidification. In this study, the seasonal variation of surface pH in IO and its long-term changes are studied, over 8 different IO bio-provinces. A rise in acidification rate over IO has been found, using 50 years of model data along with observations, which has also been asserted by a high correlation between sea surface temperature (SST) and pH. The study helps to quantify the individual contribution of factors causing this decrease in pH and identify acidification hotspots. It is found that dissolved inorganic carbon and SST dominate the seasonal variation of pH and counterbalance each other.

1 Introduction

Carbon dioxide (CO_2) is one of the most critical greenhouse gases in the atmosphere, contributing to global warming (H.-O. Pörtner et al., 2022). Atmospheric CO_2 levels are increasing at an alarming rate, especially in recent years, and have grown by 45% compared to the levels during the pre-industrial era(Petit et al., 1999). Since the industrial revolution, the atmospheric CO_2 level has been amplified from 280 parts per million by volume (ppmv) to nearly 420 ppmv as of 2021, as observed by the Mauna Loa observatory (Friedlingstein et al., 2019; Peters et al., 2007; Le Quéré et al., 2018; Sabine et al., 2004). Extensive fossil fuel emission, deforestation, land-use land-cover change (LULC), and cement production are the major driving factors for this unprecedented increase in atmospheric CO_2 (Le Quéré et al., 2018).

The misappropriations of the total emitted CO_2 by anthropogenic activities and the build-up of atmospheric concentrations are explained by the sinks offered by the terrestrial biosphere and the

oceans. Global oceans are an essential sink of anthropogenic CO_2. Oceans sequestrate nearly one-third of the contemporary anthropogenic carbon(R. Wanninkhof et al., 2013). Without oceans, the existing carbon concentration in the atmosphere would have been larger by an additional 25-30% than what we see today, and global climate change would have been much faster than what we observe (Gattuso et al., 2015; Le Quéré et al., 2018).

The natural sequestration of atmospheric CO_2 by the ocean comes at the cost of critical changes in the chemical properties of the ocean, namely the acidity (expressed as pH), alkalinity, and dissolved carbon concentrations(Rhein et al., 2013). A decreasing trend in the pH of the oceans is observed globally (Takahashi et al., 2014), and various literatures have documented its adverse impacts on disrupting the global marine ecosystems as well as reducing the efficiency of the ocean CO_2 sink (Doney et al., 2009; Egleston et al., 2010; Guinotte & Fabry, 2008; Hönisch et al., 2012; Sabine et al., 2004; Sreeush et al., 2019).

Atmospheric CO_2 dissolves to the ocean's surface depending on CO_2 dissolution conditions of the water determined by the temperature, salinity, alkalinity, dissolved inorganic carbon concentration, and other minor ions present, such as borate (Sarmiento & Gruber, 2006). Upon dissolution, CO_2 gets converted into unstable carbonic acid ($H_2CO_3^*$). The carbonate chemistry in the ocean can be simplified by following three reactions: (a) a reaction of CO_2 with water to produce $H_2CO_3^*$, (b) the first ionization of H_2CO_3 to form bicarbonate ions (HCO_3^-), and (c) a second ionization process to convert bicarbonate ions into carbonate ions (CO_3^{2-}) (Egleston et al., 2010). As a result, additional two H^+ ions are released into seawater by the second and third steps above, resulting in net ocean acidification. At the same time, H^+ions released in the first ionization process combine with the natural carbonate ions in seawater to form bicarbonates. Hence, this carbonate 'buffer' offers a resistance to change in pH due to the CO_2 dissolution.

However, a high amount of CO_2 dissolution into oceans results in decreased buffering action, thereby amplifying ocean acidification (Egleston et al., 2010; Feely et al., 2009). Another major consequence is the consumption of carbonate ions by the excess H^+ ions released due to acidification affecting the biological processes. For example, the calcifying organisms combine calcium (Ca^{2+}) arrived from weathered calcium-silicate rocks with the carbonate ions to form calcium carbonate ($CaCO_3$), which is an important part of their shell formation (Feely et al., 2009). Thus, we must understand the process of acidification on a global and regional scale by deducing the controlling factors contributing to these changes(Chakraborty et al., 2021; Sreeush et al., 2019).

Indian Ocean (IO; 30°E-120°E, 40°S-30°N) is a mild sink of atmospheric CO_2 with -0.32±0.06 (Sarma et al., 2013), -0.12±0.12 (Landschützer et al., 2016), -0.28±0.18 (V Valsala & Maksyutov, 2010) and -0.24±0.12 (Takahashi et al., 2009) petta gram carbon (PgC) yr^{-1}. The spatio-temporal variability of inorganic and organic carbon is controlled by both the physical (reversal of winds, vertical mixing, coastal and open ocean upwelling, downwelling) and biological processes (solubility and biological pump)in the ocean (Schott & McCreary, 2001; Sharada et al., 2008; Sreeush et al., 2018; V. , Valsala & Maksyutov, 2013; Vinu Valsala et al., 2012). The ocean processes associated with the solubility pump primarily drive the southern subtropical IO carbon sink, whereas the 40°S-55°S region is driven by both biological and solubility pumps equally (Vinu Valsala et al., 2012). The interannual variability of IO sea-to-air CO_2 fluxes has dominant variability in the south-eastern subtropical IO associated with IO Dipole (IOD, Vinu Valsala et al., 2020). The dynamics of ENSO and IOD play a significant role in sea-to-air CO_2 flux variability in the western boundary of the IO along with upwelling and eddies(Sreeush et al., 2018, 2020; V. , Valsala & Maksyutov, 2013; Vinu Valsala & Murtugudde, 2015). The tropical IO alone

contributed to sinking 16.6±5.1 PgC of anthropogenic carbon amounting a 16% of the global ocean sink (Key et al., 2004; Sabine et al., 2004).

Substantial seasonal variability and 0.07 units drop in pH over the last 50 years can be observed in the Western Arabian Sea (WAS) (Sreeush et al., 2019). (Chakraborty et al., 2021) demonstrated the dominant seasonal cycle in the surface ocean pH of the Arabian Sea and Bay of Bengal (BoB) in terms of those driven by surface ocean temperature, dissolved inorganic carbon content, surface ocean alkalinity, and salinity. The western IO acidifies faster, with 16% of it exacerbated due to the SST warming alone (Sreeush et al., 2019). However, the former looked at the seasonal cycle of the northern IOand and its controlling factors. The latter looked at trends in acidification focussed only on the WAS. This work's primary motivation is the lack of understanding of the region-specific spatio-temporal trends of pH and its causing factors in the entire IO. For example, the direct measurements of boron isotopes in the Minicoy coastal waters of the Arabian Sea and deduced pH values for the past 16 years indicate large interannual pH fluctuations obscuring the long-term trends (Tarique et al., 2021).

This study aims to understand the controlling factors of the seasonality of pH and its trends over the IO bio-provinces via observations, biogeochemical model outputs, and climate model simulations. The biophysical interactions over each bio-provinces are unique, which has a significant impact on regulating the surrounding ocean pH. The strength of the solubility and biological pump to sequestrate the atmospheric carbon by transporting it to the deep ocean, varies across each bio-provinces. As pH depends on the biogeochemistry largely, Eight IO bio-provinces categorized on the seasonal variance in chlorophyll imparted in the form of Net Community Production depth as in (Sreeush et al., 2020), were utilized in this study (supplementary Text S1 and Figure S1). The individual contribution from the major physical factors such as Sea Surface Temperature (SST), Dissolved Inorganic Carbon (DIC), Alkalinity (ALK), and Salinity (S) to the seasonal pH variability and its trend are investigated for each bio-province. The rest of the paper is organized as follows. Section-2 introduces the data and methodology. Section-3 presents the results and discussions, followed by a summary in Section-4.

2 Materials and Methods

We used model outputs from OTTM-BGC (Ocean Tracer Transport Model-Biogeochemistry: Sreeush et al., 2018, 2019, 2020; V Valsala & Maksyutov, 2010; Vinu Valsala et al., 2008) and ROMS (Regional Ocean Modeling System: Chakraborty et al., 2018, 2021).

2.1 OTTM-BGC

OTTM is an offline model coupled with OCMIP-II (Ocean Carbon-Cycle Model Inter-comparison Project – II) biogeochemistry model as in (V Valsala & Maksyutov, 2010; Vinu Valsala et al., 2008), further developed with a modified parameterization for the community compensation depth with a spatio-temporal dependency on satellite-derived surface ocean Chl-a seasonality and a time-varying penetrative short-wave radiation by (Sreeush et al., 2018, 2019, 2020). The model dynamics are prescribed from GFDL (Geophysical Fluid Dynamics Laboratory) re-analysis data via three-dimensional currents (U, V), temperature, salinity and two-dimensional mixed layer depth, evaporation and precipitation rates, surface heat flux, surface wind stress, and sea surface height. The zonal and meridional resolutions are 1^o x 1^o with 360 grid points longitudinally and latitudinally at higher latitudes and a finer resolution of 0.8^o at the equator. The vertical and

horizontal mixing is resolved via KPP(Large et al., 1994) and Redi diffusion(Redi, 1982), respectively. The biogeochemical model coupled to OTTM is based on the OCMIP-II protocol, which uses a nutrient restoration approach for biological production with phosphate as its basic currency(Najjar & Orr, 1998). The DIC and ALK computation in the model are linked to the phosphate and calcium cycling via the Redfield ratio(Anderson & Sarmiento, 1994; Najjar & Orr, 1998). Further details of the model are provided in (Sreeush et al., 2018, 2019). The simulations from 1990-2010 have been used in the validation and seasonality analysis and from 1961-2010 for trend analysis.

2.2 ROMS model outputs

A high-resolution coupled ocean-ecosystem model configured using the Regional Ocean Modelling System (ROMS) simulated outputs are utilized to compare the results retrieved from the OTTM-BGC model for 1990-2010. The physical model is configured with a horizontal grid resolution of 1/12°, and it carries 40 vertical layers in a terrain-following s-coordinate system. The K-Profile Parameterization (KPP; Large et al., 1994) scheme is used for surface ocean vertical mixing parameterization. Biharmonic viscosity and diffusion schemes are chosen for horizontal mixing (Griffies & Hallberg, 2000). Surface heat and momentum fluxes are internally calculated by ROMS using the bulk parameterizations (Fairall, et al., 1996; Fairall, et al., 1996; Liu et al., 1979) The biological component of the model uses the nitrogen cycle model with parameterized sediment denitrification as described by (Fennel et al., 2006). The time rate of change of concentration of each state variable describes the balance of advection-diffusion and source-sink terms among the nitrogen cycle-related state variables (Fennel et al., 2006). The biological model resolves the oceanic carbon cycle. The model carbonate chemistry in the biological model is described in (Fennel et al., 2008; Zeebe & Wolf-Gladrow, 2001), and (Laurent et al., 2017). The oceanic carbon cycle is represented in the model using four state variables viz. alkalinity, dissolved inorganic carbon, large and small detritus class with carbon concentration. Dissolved inorganic carbon dynamics include the primary production, respiration as a sink, and source term, respectively, following Redfield stoichiometry besides gas exchange at the air-sea interface. The biogeochemical processes, such as calcite formation and dissolution, nitrate uptake and regeneration, and sulfate reduction, are represented in alkalinity dynamics. The increasing trend of atmospheric pCO2 is prescribed in the model. Air-sea gas exchange is prescribed following (Rik Wanninkhof, 2014). The detailed model configuration can be found in (Chakraborty et al., 2018, 2021).

2.3 CanESM2 model outputs

The historical model output from the second generation Canadian Earth System Model (CanESM2) is compared with the OTTM pH, DIC, and ALK data for the period 1961-2005 for the eight regions. CanESM2 (Barker et al., 2008; Li & Barker, 2005; von Salzen et al., 2005), being part of the CMIP5 project, has an AGCM of T42/T63 spatial resolution and 35 vertical levels coupled with an OGCM of 256 x 192 resolution and 40 levels in-depth, along with a sea-ice model. The Canadian Model of Ocean Carbon (CMOC) is used with CanESM2 to simulate the oceanic carbon cycle (Zahariev et al., 2008). The solubility pump follows the OCMIP-II protocol, whereas the biological pump involves time-dependent variables such as DIC and Alkalinity, which are determined using a constant Redfield ratio. The model has nitrogen as its basic currency.

2.4 Observational Dataset

Climatological surface pH observations from (Takahashi et al., 2014) are utilized to validate the model outputs. These datasets are retrieved via statistical interpolation of multiple ship observationsfrom1990s to 2010. (Takahashi et al., 2014) dataset provides global coverage with a 4^o x 5^o via linear interpolation method. The data link is provided in the Data availability section.

2.5 Sensitivity of SST, S, DIC and ALK on pH seasonality and trends

Change in surface pH is a function of DIC, SST, ALK and S, which are its prominent contributors (Takahashi et al., 2009; Vinu Valsala & Murtugudde, 2015). There are other constituent factors such as sulfate, phosphate, borate, and fluoride, whose contribution to change in pH is negligible (Hagens & Middelburg, 2016). To quantify the impact of the prominent contributors, we can rewrite pH variability, as implemented in (Sreeush et al., 2019):

$$\frac{dpH}{dt} = \frac{\partial pH}{\partial SST}\frac{dSST}{dt} + \frac{\partial pH}{\partial DIC}\frac{dDIC}{dt} + \frac{\partial pH}{\partial ALK}\frac{dALK}{dt} + \frac{\partial pH}{\partial S}\frac{dS}{dt} + (other\ minor\ ion\ contributions) \quad (2.1)$$

The pH was reconstructed, referred to as CTRL using the above equation and the OCMIP- II protocol. The time-varying temperature and salinity were obtained from GFDL reanalysis data (Chang et al., 2013), whereas DIC and Alkalinity were obtained from OTTM model runs. Minor influencers like sulfate, phosphate, borate, and fluoride are residuals. The root means square difference (RMSD) between the recalculated pH (CTRL) and model pH is examined and ensured that bias is within ± 0.005 pH, much less than the dominant variabilities in each of the terms in Eq. (2.1).

To quantify the individual impact of SST, S, DIC and ALK on pH seasonality and trends, we carried out experiments referred to as sensitivity experiments (from now on referred to as SENS). In this method, each variable of interest in eq. (2.1) is suppressed into climatological annual mean values (derived from 1990 to 2010) while others are unchanged. It was repeated for all the variables of interest one at a time, thereby giving the effect of SST, S, ALK and DIC on pH seasonality via CTRL and SENS difference. A similar approach has been considered for the pH trend analysis. Here, each of the variables of interest is de-trended individually. Others remain unchanged and then utilized for pH reconstruction. The CTRL and SENS difference gives the effect of trends in these variables into the net trend of the pH. The results are presented as area-averaged over each bio-province.

3 Results and Discussion

3.1 Validation of OTTM and ROMS model pH with observation

This section gives a detailed validation of OTTM and ROMS simulated pH with (Takahashi et al., 2014). Supplementary Figure S2 shows the annual mean surface pH of the IO from the synthesis of (Takahashi et al., 2014). Overall, the IO has a lower pH value than the global oceans, indicating a high DIC from the upwelled waters (Chakraborty et al., 2021). The WAS has low pH, and the coastal regions also show a significant pH variation than open waters. In the oligotrophic gyre, the

241 pH is slightly stronger indicative of less DIC and low acidity (Vinu Valsala et al., 2012). The
242 spatial variability of pH indicates the necessity to consider regions separately to understand the
243 controlling factors better.RMSD calculated between model simulation and CTRL (reconstructed
244 pH) over the IO is overall very small, especially in the Southern IO, about 0.004, whereas RMSD
245 in the Northern IO varies from 0.007 to 0.014 (supplementary Figure S3).
246

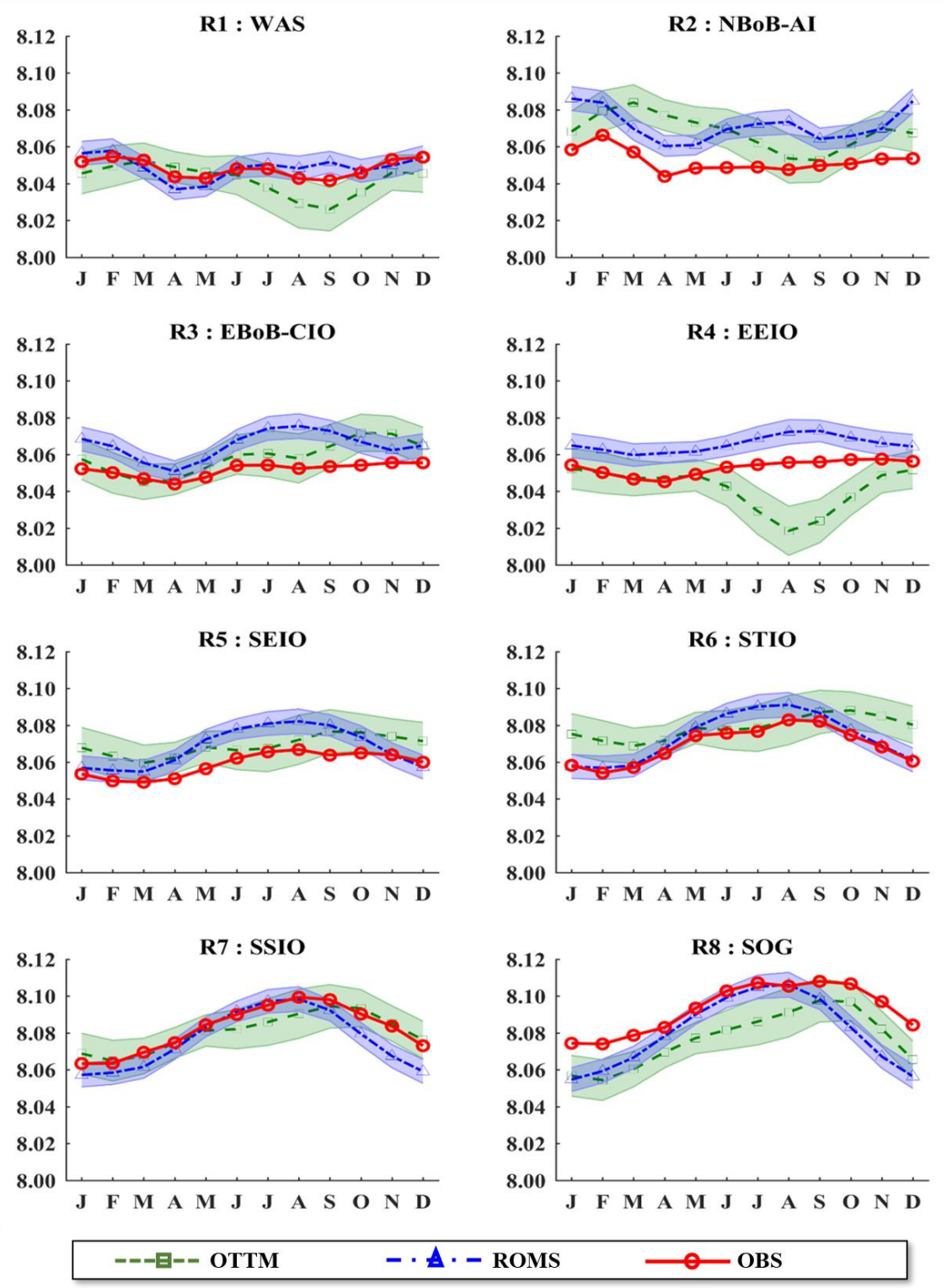

Figure 1: Comparison of area-averaged model pH (OTTM-green dash-dot line and ROMS-blue dotted line) with that of (Takahashi et al., 2014)**; red line, observations for 8 IO bio-provinces. Error bars show standard deviations of individual months over different bio-provinces from 1990 to 2010.**

Both OTTM and ROMS simulations reasonably capture the pH seasonality compared with the observation (Figure 1). In WAS, during the pre-monsoon season, the SST warming increases the concentration of H+ions, leading to surface ocean acidification. The same can be seen in observation and models during April-June (AMJ). Also, the model pH tends to be more acidic during the summer monsoon than in observation. One reason may be due to strong upwelling during the summer monsoon in the model. ROMS pH conforms well to observation with slight alkaline bias during August-September. The dip in pH during March-May (MAM) in the NBoB-AI, as seen in observation, is not well captured by ROMS (Figure 1). Strong stratification might suppress the entrainment of DIC into surface water, making pH tend towards alkaline. The riverine input of dissolved carbon can also influence BoB acidification, which is not represented well in models (Rao & Sarma, 2022). In EBoB-CIO, OTTM pH overestimates from June to December by 0.008-0.018 units than observation. Similarly, ROMS pH is more alkaline during the summer monsoon, where the bias peaks at around 0.025 units. The effect of colder SST from the western part of this region may make the pH less acidic. In EEIO, OTTM is more acidic during the summer monsoon by a margin of 0.03 units compared to observation. One reason can be the dominance of the effect of DIC during the summer monsoon season. However, ROMS seasonality can be seen matching observation with a slight bias. In the Southern IO region,i.e. SEO and STIO, OTTM pH seasonality matches reasonably well with observation, with a slight bias of around 0.018 units. In SEO, ROMS has a slightly alkaline bias of around 0.02 units during the summer monsoon. The seasonality of pH of both models (OTTM and ROMS) in SSIO and SOG matches very well compared with observations.

3.2 Control of SST, DIC, ALK and Salinity on a seasonal pH cycle over the IO

The seasonal cycle of pH and its sensitivity by changes in SST, DIC, ALK and Salinity is retrieved by subtracting the pH from the control and sensitivity runs (see section 2.5 and Figure 2). The results are summarized for eight bio-provinces in the following sub-sections.

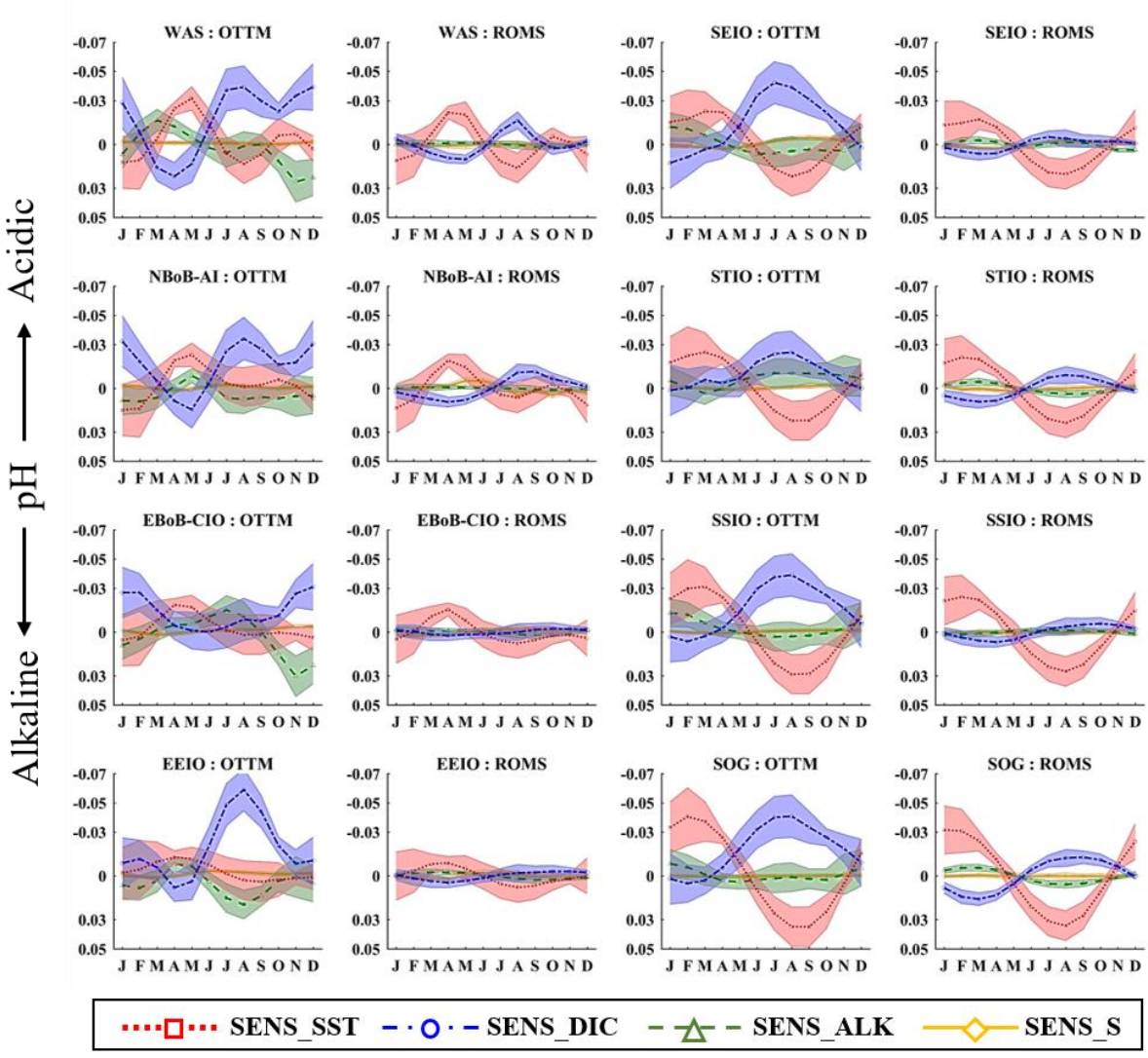

Figure 2: Difference between CTRL and SENS for each SST, DIC, ALK, and S, respectively. The shaded error bar indicates standard deviations of individual months over-identified bio-provinces in the IO from 1990 to 2010 using OTTM and ROMS datasets.

3.2.1 WAS and NBoB-AI region

In WAS and NBoB-AI regions, it is observed that warming of SST during the pre-monsoon (AMJ) and post-monsoon (ON) causes the pH to be more acidic while cooling during the summer monsoon makes it less acidic, caused by the SST component (Cao et al., 2007; Chakraborty et al., 2021; Kapsenberg et al., 2017; Zeebe, 2012). An increase in temperature causes dissociation of carbonate species, releasing excess protons. Temperature-dependent dissociation constants further accelerate this dissociation rate (Cao et al., 2007; Zeebe, 2012). In both the regions during pre-monsoon, an increase in pH value is caused by DIC components. It is attributed to the poor mixing conditions in the extremely warm SST during this part of the season. The biological sink in the surface zone consumes the DIC and has no replacement/replenishment of DIC due to weak mixing.

DIC decreases pH in the summer monsoon (July-September), acidifying the waters. Upwelling in the WAS causes DIC to increase during the summer monsoon and, subsequently, acidification (Chakraborty et al., 2021; Fassbender et al., 2011). Alkalinity in WAS contributes to acidification during JFM and AMJ seasons, as observed in (Sreeush et al., 2019), whereas, in NBoB-AI, it acidifies pH during pre-monsoon.

3.2.2 EBoB-CIO and EEIO

Similarly, in the EBoB-CIO region, warming of SST makes pH acidic during pre-monsoon. However,post-monsoon SST shows a negligible effect on the seasonality. This bio-province extends to the central BoB and central equatorial IO. A part of this region appears to be warmer SST conducive to atmospheric convection, and the western part of this region shows colder SST. The contribution of DIC in acidifying pH is more than the contribution of SST. During the winter monsoon, north equatorial currents follow westerlies (Schott & McCreary, 2001), whereas, during spring and fall, the Wrytki-jets are eastward. The boreal summer monsoon currents are also eastward. It is observed that whenever the currents are eastward, the DIC has a limited role in the seasonality of surface ocean pH. However, when the currents follow westerlies, DIC acidifies pH. Alkalinity, in this region, acts as a strong counterbalance to DIC during JFM and OND (October-December) seasons.

In EEIO, SST increases (decreases) pH in JFM (AMJ) season. It is attributed to seasonal variations of SST along the equatorial ocean belt, as discussed in (Dommenget, 2011; Donguy & Meyers, 1996). The most significant contribution of DIC in acidifying pH, specifically during the summer monsoon, is noted when the currents are strongly eastward. Alkalinity provides considerable buffer action against acidifying pH throughout the season for EEIO.

3.2.3 Southern IO (SEIO, STIO, SSIO and SOG regions)

The behavior of pH sensitivity by changes in SST (SENS_SST) is significantly different in the Southern IO and the subtropical oligotrophic gyre region compared to WAS, BoB and the northern IO. The seasonality of pH in the SEIO and STIO regions is similar. The amplitude of the SENS_SST time series is higher in SSIO and SOG than in the previously discussed regions. Since these are wind-driven circulation regions, the warming and cooling of SSTplay an important role in pH seasonality (Cao et al., 2007; Kapsenberg et al., 2017; Zeebe, 2012) The dominance of SST in the seasonal pH cycle in these regions indicates a clear role of the solubility pump in the carbon cycle than the biological pump (Vinu Valsala et al., 2012). If DIC is suppressed, the pH will tend towards basicity in the Southern IO and the Subtropical gyre region. This trait is observed from AMJ till OND seasons. It can be explained by the mixed layer deepening of these regions during austral winter. The deepening of the mixed layer entrains the subsurface DIC to the surface, thereby enhancing pH seasonal cycle. The maximum enhancement happens in the southernmost regions where mixing is further expected to be dominant. Buffer action from Alkalinity is observed in the SEIO region. The role of alkalinity in the IO Subtropical gyre region is not so significant.

The influence of each component, i.e. SST, DIC, ALK and S, on pH for each month has been summarized in terms of seasonal mean contribution in Table S1 and S2 (refer to Supplementary Information) for OTTM and ROMS, respectively. Noticeably, as shown in Table S1, in SEIO, DIC contributes to acidity throughout the year, except for JFM. Alkalinity promotes acidification only during JFM. Thus, a weak seasonal counterbalance is observed between DIC and ALK in this region. Like SEIO, a similar seasonal pattern is observed in SSIO and SOG, respectively, but it is very weak. The effect of salinity on the seasonality of pH in all bio-provinces is quite negligible.

It is evident from the impacts of each of the controlling factors such as SST, DIC, ALK and S on the seasonality of pH of various regions of the IO that the effects of SST and DIC are mutually correlated and opposite to each other. These results are in agreement with studies like (Midorikawa et al., 2010, 2012) in the western North Pacific and Pacific sectors of the Southern Ocean, respectively, (Bates et al., 2012) in the North Atlantic Ocean, and (Sreeush et al., 2019) in the WAS. It can be attributed to an increase in SST, causing the surface ocean to be more stable and resist mixing, which causes depletion of DIC by a biological pump with fewer chances of replenishment of dissolved H^+ions. Therefore, when SST contributes to an increase in seasonal amplitudes of pH, the DIC'scontribution is to decrease it. On the other hand, the SST cools and reduces the pH by releasing fewer H+ ions when the mixing is deeper. At the same time, the increase in enrichment of DIC by deep water mixing causes enhancement of pH (acidity). In upwelling seasons, this mechanism further intensifies (Fassbender et al., 2011). Alkalinity itself is a function of biology. When soft tissue pump happens, alkalinity increases, while hard tissue pump causes a decrease in alkalinity. Therefore, the role of alkalinity in surface ocean pH seasonality is interlinked with both biological and solubility pumps (Chakraborty et al., 2018, 2021).

The seasonality of pH in ROMS (summarized in Table S2) matches well with OTTM, though we observe a slight bias in the amplitude of all SENS variations. In OTTM, we observe that SST and DIC are the two major influencers in acidifying surface pH. These drivers are well entwined and subdue the effect of each other. Seasonality of SST is well observed in both models, especially in the Southern IO, where these wind-driven regions are dominated by strong solubility pumps rather than biological pumps (Vinu Valsala et al., 2012). It can be observed that DIC in ROMS is underestimated in all regions compared to OTTM. One reason is biological pump underperforming in these regions. The seasonality contribution of ALK and S to acidification in ROMS simulation is insignificant.

3.3 Sensitivity of SST, DIC, S, ALK on the trend of pH

The percentage contribution of SST, DIC, ALK and S on the net trend of pH is depicted in Figure 3, and the respective values are listed in Supplementary Table S3. The IO has acidified from 8.132 in 1961 to 8.064 units in 2010. A decrease of 0.0675 units in the last 50 years is attributed to changes in DIC (69.28%), followed by a 13.82% temperature contribution. Alkalinity and salinity contribute by 7.12% and 2.76%, respectively, insignificant compared to DIC and SST. Various other studies (Fine et al., 2017; Waters et al., 2011) have also estimated that the average ocean pH has decreased by 0.063 over 35 years, with temperature and salinity contribution varying between 1.6 to 16% of the total.

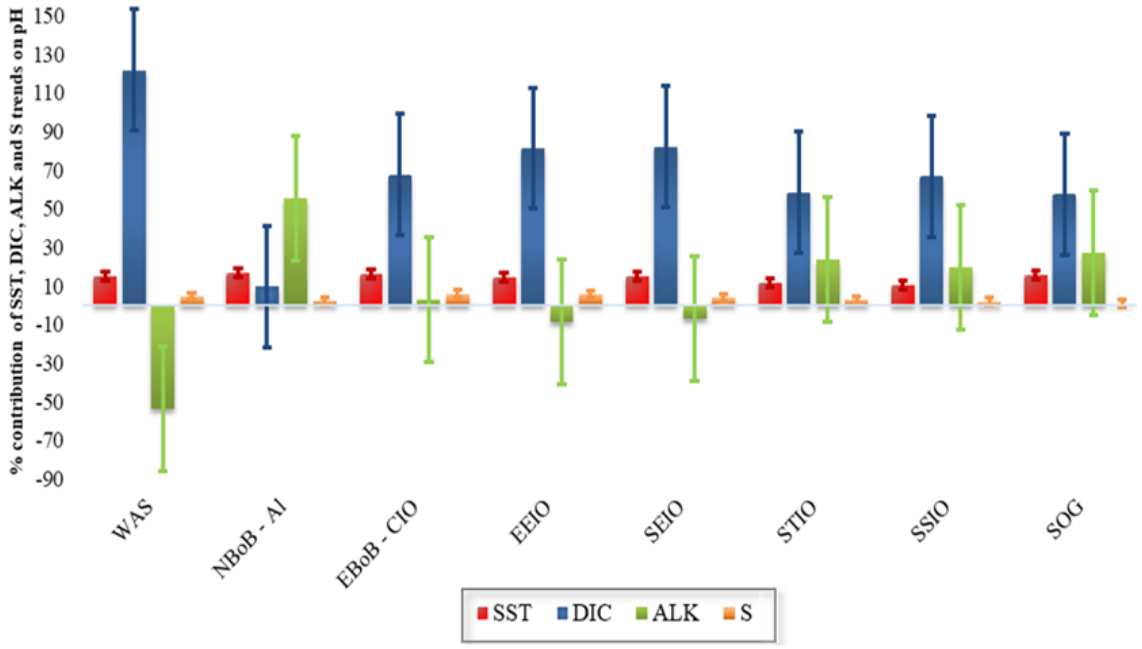

Figure 3: Percentage contribution of SST, DIC, ALK and S on the net trend of pH with error bars showing standard deviation for each bio-provinces.

pH has decreased by 0.064 units in the WAS region in 50 years. As seen in Figure 3, DIC is the most dominant driver of interannual pH variations over WAS (121.8%). The likely reason behind this is that WAS is a strong upwelling coastal region, thereby having a high DIC concentration. A similar inference has been reported by (Fassbender et al., 2011) for the upwelling regions of the California coast. However, the influence of alkalinity is -53.4%, which indicates that the buffering of the ocean carbon chemistry regulates the change in pH due to the increased dissolution of atmospheric CO_2 (Sreeush et al., 2019). DIC/ALK ratio is found to be high for the Arabian Sea (around 0.86), which supports our finding of high buffering action of alkalinity in this region (Sabine et al., 2002). The reason explained in (Sabine et al., 2002) is that the prominent upwelling in this region gets the high buffer capacity (high DIC/TA) water from the deep ocean to the surface. The role of temperature results in a 15.1% increase in acidity, and it is consistent with the 15.6% contribution of warming over pH as identified by (Sreeush et al., 2019). Salinity contributes about 4.69% to the decrease in pH.

The pH in the NBoB-AI has decreased by 0.06 units from 8.129 in 1961 to 8.069 units in 2010, comparable to (Sarma et al., 2013). Coastal ocean dynamics strongly dominate the variability of this region, and the physical, chemical, and biological conditions are different from other regions. It can be inferred from the trend analysis that the pH trend is mostly dominated by alkalinity in this region (55.6%), followed by SST (16.08%). It is interesting to note that the overall contribution of alkalinity is to decrease the pH over 50 years, contrasting with the buffering action of carbonate chemistry as seen in WAS. With DIC and salinity contributing only 9.7% and 2.12%, respectively, it is understood that the pH decrease in this region can be attributed majorly to the interplay between alkalinity and SST.

The contrasting behavior, which indicates that alkalinity increases the acidification, can also be observed in the seasonality analysis. In Figure 2, NBoB-AI, the alkalinity is seen to be contributing to increased acidification in the pre-monsoon months. Similar behavior of alkalinity has been observed by (Kapsenberg et al., 2017) in the Bay of Villefranche-sur-Mer, France and (Luchetta et al., 2010) in the northern Adriatic Sea.

In EBoB-CIO, DIC contributes about 67.78% to pH change. Coastal upwelling during summer monsoon increases the DIC content, thus affecting the pH (Fassbender et al., 2011). It is followed by temperature, contributing about 16.08%. Similar to NBoB-AI, no buffering of pH by alkalinity is seen in this region, contributing to a 2.9% increase in pH. Salinity contributes about 6% to acidifying the water. From 8.119 in 1961 to 8.06 units in 2010, pH has decreased by 0.06 units in the last 50 years.

A similar trend is observed in the Eastern and Southern Equatorial IO as in WAS. EEIO has acidified by 0.069 units, while SEIO has acidified by 0.065 units in the last 50 years. Both the regions have a high DIC contribution of 81.38% (EEIO) and 82.15% (SEIO) in the pH trend, followed by a contribution of temperature at 14.7 % and 15.23%, respectively. Similar results in the EEIO region have been reported in (Xue et al., 2014). EEIO and SEIO lie exclusively in the Indo-Pacific Warm Pool region, analogous to very high SST, more than 28^{o}C throughout the year (de Deckker, 2016). Higher the SST, the acidification rate is also faster. The southeast monsoon around the West Pacific follows the trade winds, which causes coastal upwelling along the coast of Java-Sumatra from June-September (Horii et al., 2016; Susanto et al., 2001). It causes subsurface cooler water to entrain into warmer surface waters (Bray et al., 1997), replenishing it with nutrients. We have found a significant relationship while observing the seasonality contribution of DIC in pH during this period in EEIO (as in Figure 2). As seen in WAS, upwelling causes subsurface DIC to rise, causing pH to acidify further. (Xue et al., 2014) argued that the increase in DIC in EEIO is due to this region being a CO_2 source and outgassing CO_2 reversal increasing the surface DIC. We observe the buffering action of alkalinity in both regions, but it is rather weak, with EEIO and SEIO regions having -8.32 % and -6.85% contributions, respectively. The contribution of salinity, 5.88% (EEIO) and 3.96% (SEIO), is also weak.

The Southern Tropical and Subtropical IO are acidified more than the tropics. STIO has acidified by 0.068 units, SSIO by 0.072 units, whereas SOG acidified by 0.071 units in the last 50 years. The major reason is the lack of calcium/magnesium concentration in open ocean regions (Duarte et al., 2013). We observe that DIC is the dominant contributor with 58.45% in STIO, 66.75% in SSIO and 57.49% in SOG regions, respectively. The buffer action of Alkalinity is absent, with ALK contributing positively in these regions, i.e., 23.55% (STIO), 19.79% (SSIO), and 27.23% (SOG). A similar inference has been drawn by (Takahashi et al., 2014), wherein biological differences in various parts of the IO significantly affect carbon chemistry. It is followed by SST, contributing 11.35% (STIO), 10.21% (SSIO), and 15.47% (SOG) in these regions. The contribution of salinity is not significant.

In a similar line of approach, (Kapsenberg et al., 2017) identified the factors influencing ocean acidification, and their contribution was computed using a similar sensitivity analysis methodology (alternately called here deconvolution of time series). Trend analysis at 1 m depth yields that the pH trend decreased (-0.0028 units yr^{-1}), whereas Alkalinity ($+2.08$ μmol kg-1 yr^{-1}), DIC ($+2.97$

μmol kg−1 yr^{-1}) and Temperature anomaly trend increased (0.072 ◦C yr^{-1}). Deconvolution analysis at 1 m depth evaluated that the collective contribution of DIC and alkalinity was 59 %, whereas warming contributed 41%. The contribution of salinity was nil. Further, results showcased that alkalinity and DIC trends are more distinct at the surface. Another study in the northern Adriatic Sea (Luchetta et al., 2010) yielded similar results where pH acidified by −0.0025 units yr^{-1} but the alkalinity trend increased by 2.98 μmol kg^{-1} yr^{-1} within 75 m depth.

3.4 Comparison of ALK, DIC and pH between OTTM and Can-ESM2

The OTTM simulated DIC, pH and ALK anomaly are thoroughly compared (from 1961 to 2005) with CanESM2 (as seen in Figures4A-4C). The OTTM results are in good agreement with that of CanESM2 for all the eight regions in our study (Figure 4A). The OTTM shows an increasing trend in DIC anomaly from -0.04 (1961) to +0.04 (2005) in region-1which agrees with that of CanESM2, except between 1961 and 1966 (Figure 4A1). In NBoB-AI OTTM shows a negative anomaly from 1961 to 1966 compared to CanESM2 (Figure 4A2). Both the models are in good agreement with each other except for 1961-1966 and 1981-1986. OTTM also reproduced the variability and trend in DIC anomaly for regions 3, 4, 7, and 8 (EBoB, EEIO, SSIO, and SOG, Figure 4A3 to 4A6). For SEIO and STIO, the models are in good agreement except between 1986 and 1991. The variability in DIC anomaly is high for regions 1 to 4 compared to the other four regions. The pH anomaly shows a negative trend between 1961 and 2005 in all regions except region 8 (Figure 4B1-8). The seasonal variability in pH anomaly is higher in OTTM than CanESM2 in regions 1 to 4 (Figure 4B1-4B4), especially in the EEIO after 2001.

The ALK anomaly agrees with CanESM2 (Figure 4C1-4C8) except for region 2 between 1981 and 1986 (Figure 4C2). The variability in ALK anomaly is high for regions 2 to 4 (Figure 4C2-4C4) compared to that of other regions.

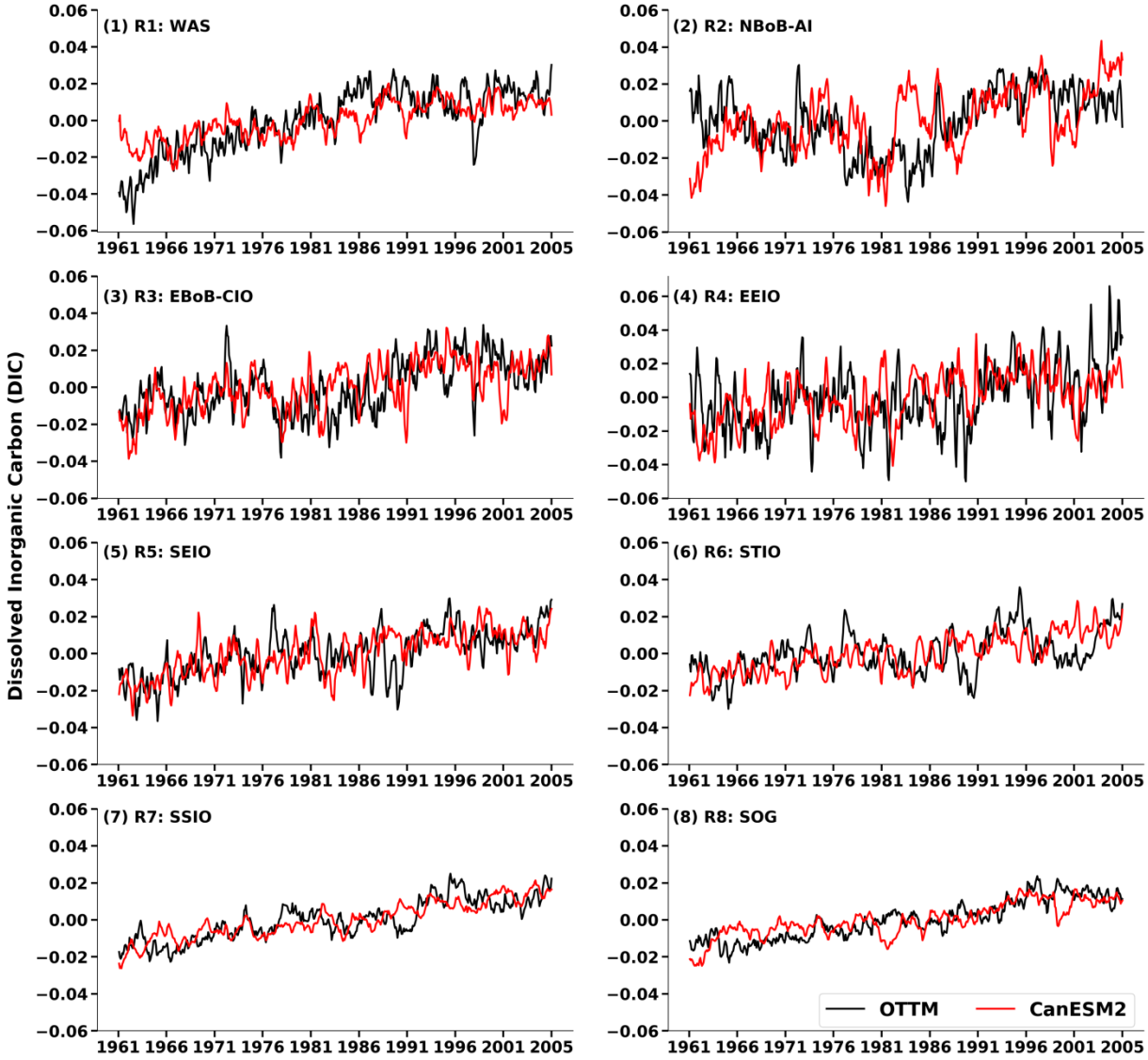

Figure 4A: OTTM (black line) DIC anomaly with CanESM2 (red line) for 8 IO bio-provinces from 1961 to 2005.

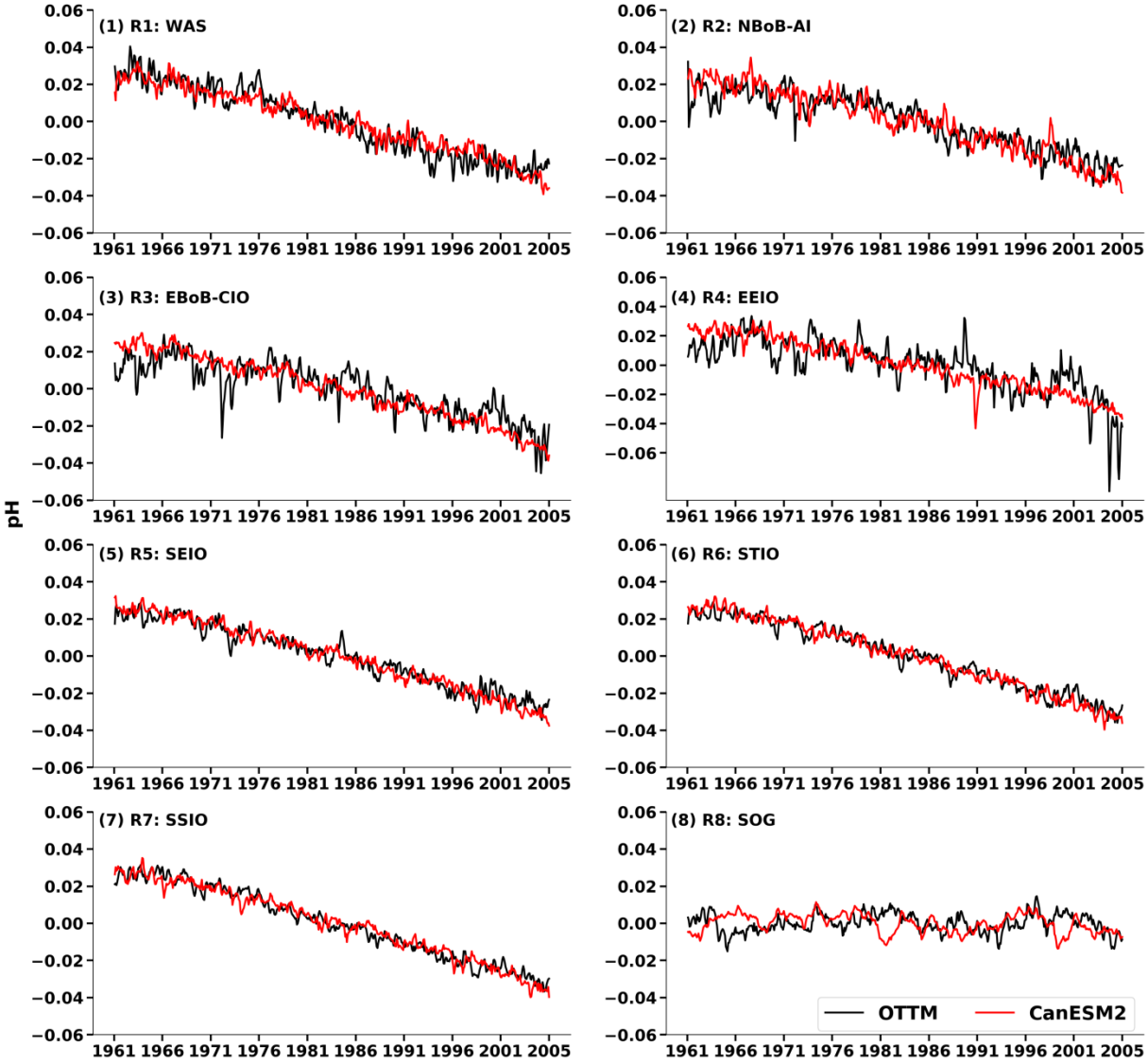

Figure 4B: OTTM (black line) pH anomaly with CanESM2 (red line) for 8 IO bio-provinces from 1961 to 2005.

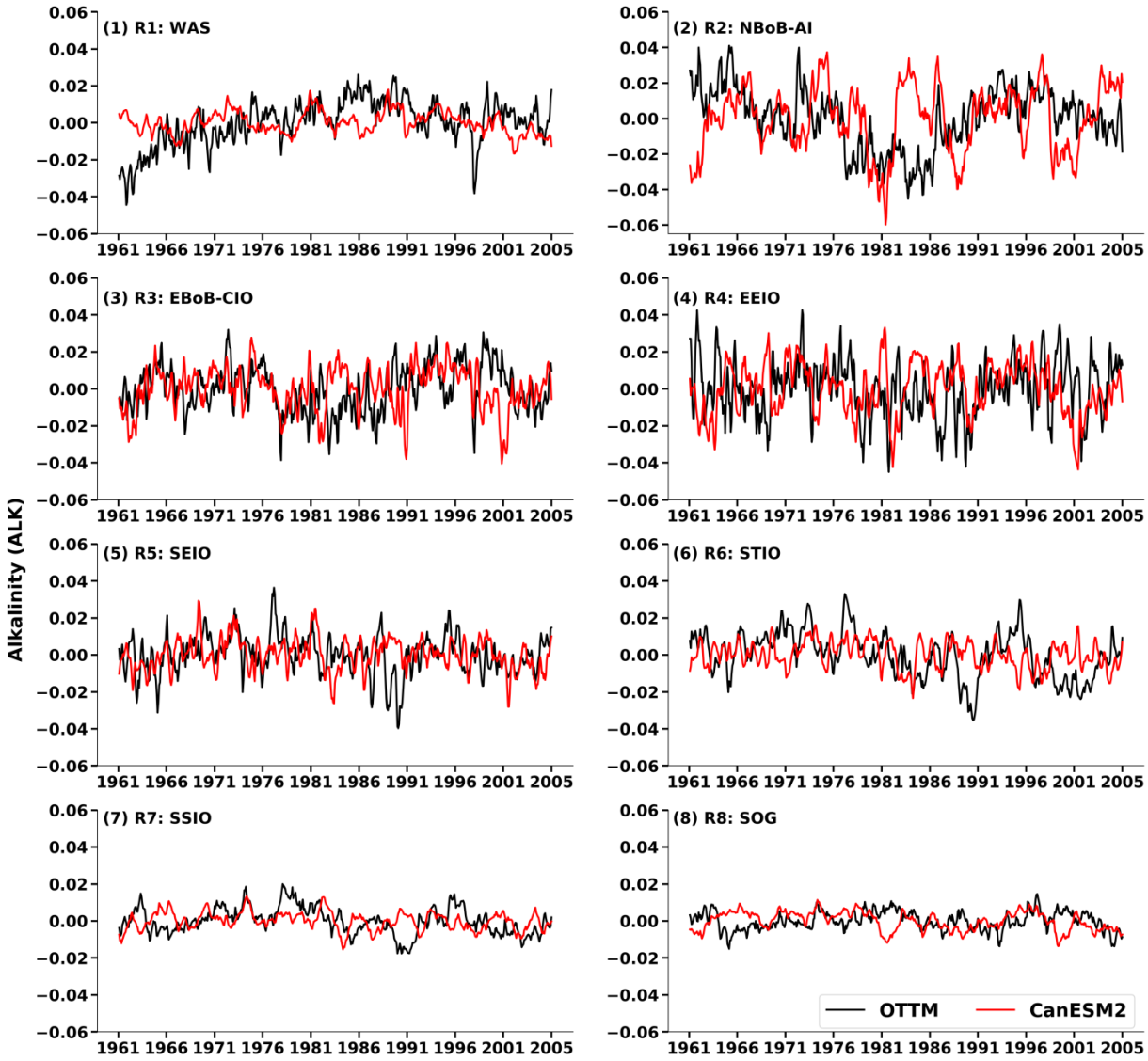

Figure 4C: OTTM (black line) ALK anomaly with CanESM2 (red line) for 8 IO bio-provinces from 1961 to 2005.

3.5 Role of ocean warming in the trend of pH

An earlier study showed that WAS warming alone contributes to ocean acidification by 15.6% (Sreeush et al., 2019). A similar analysis has been carried out for the entire IO. A trend in ocean SST (GFDL re-analysis data used to run OTTM) and trend indifference of pH between CTRL and SENS_SST has been calculated and shown as a scatter diagram for all grid points belonging to each region. The trend is analyzed for each season separately for pH. Irrespective of the decadal trends in Alkalinity or DIC, the relation between SST and pH appears robust among all the regions analyzed in the tropical IO. From Figure 5, it is clear that the ocean SST trend is negatively correlated with pH trends. It indicates that ocean warming directly enhances or accelerates ocean acidification. Strong dependence of pH on temperature has been observed in various parts of other

global oceans (Cao et al., 2007; Kapsenberg et al., 2017; Sreeush et al., 2019; Zeebe, 2012). Our analysis infers this dependency in the IO. The exact correlation values are listed in table S4 (refer to Supplementary Information).

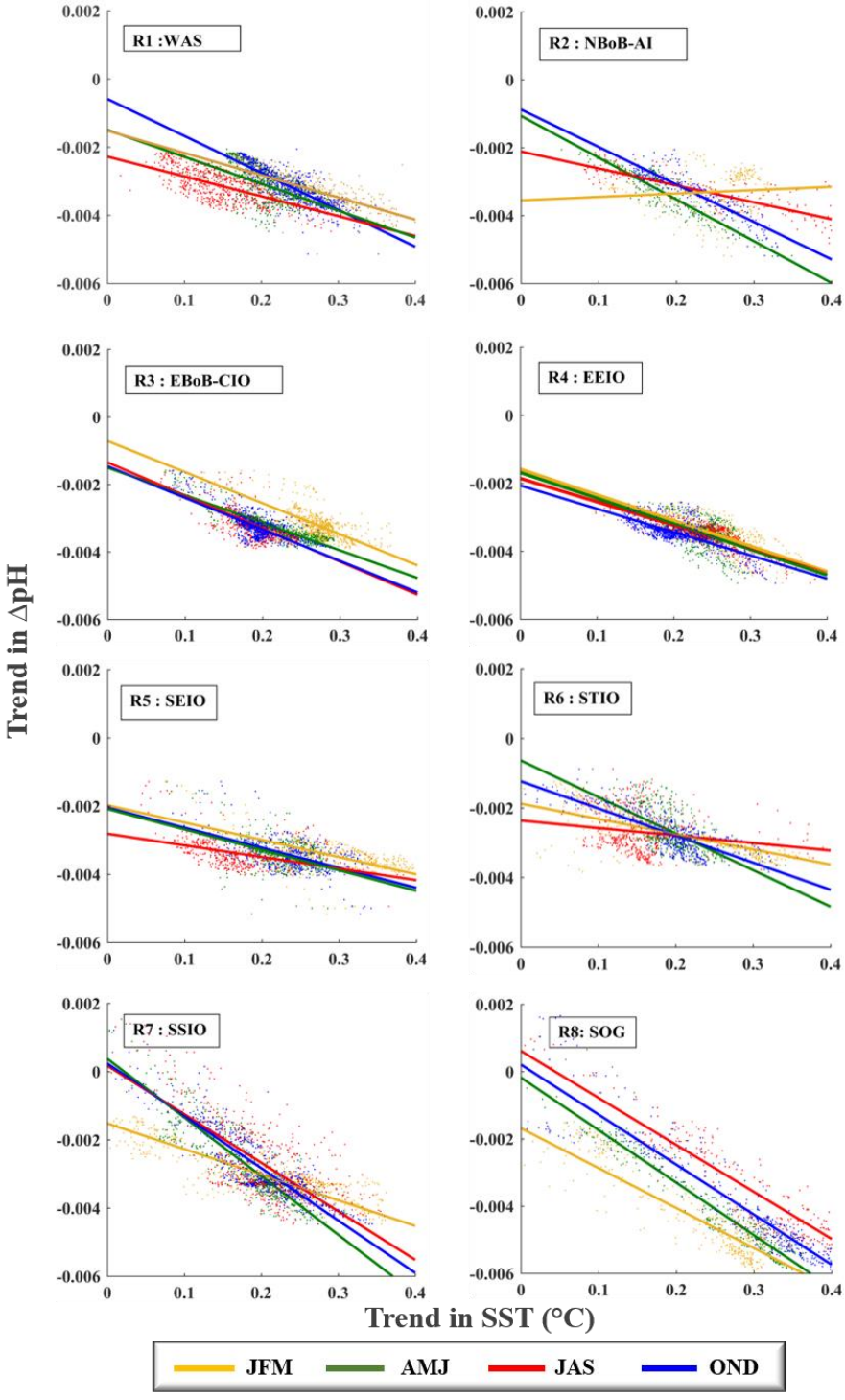

Figure 5: Scatter of trends in SST (°C) vs trends in pH (Δ pH; due to the SST alone) for JFM (yellow), AMJ (dark green), JAS (red), OND (dark blue) respectively over the study region

4 Conclusions

A detailed regional analysis of IO bio-provinces has been done in this study using model-simulated pH with realistic and controlled forcings. It is found that the contribution of DIC and SST variations dominates the changes in pH seasonality. The effect of SST and DIC are contrasting in nature, and their impacts are significantly different in the pre-monsoon and post-monsoon seasons in all the bio-provinces. The warming of SST during the pre-monsoon and post-monsoon causes pH to be more acidic, while during the summer monsoon, the decrease in SST increases the pH. The contribution of ALK and S is relatively less in the seasonality of pH variation. IO region is found to have acidified by 0.0675 pH units which are majorly attributed to changes in DIC (69.28%) followed by changes in SST (13.82%). The trend in pH is observed to be affected majorly by DIC in most bio-provinces except for the NBoB-AI, wherein ALK and SST are primary contributors. This coast-dominated region illustrates a contrasting buffer action of carbonate chemistry, and the pH decrease occurs majorly due to the interdependence of ALK over S, SST, biological and physical factors. The absence of ALK buffering acidification is also seen in the southern IO bio-provinces. Though the effect of S is comparatively less than the trend in pH in most regions, it plays a significant role in modulating the ALK variations and hence the pH. The relation between SST and pH appears robust among all the regions analyzed in the tropical IO. A strong negative correlation between SST and pH trends emphasizes the predicament of accelerated acidification of the IO basin due to the escalation of temperature owing to climate change.

Quantifying the effect of controlling factors over pH and further investigating the inter-relationships between these variables on a regional and local scale is the need of the hour to prepare better the authorities to mitigate and decelerate the adverse impacts of IO acidification. In addition to model simulations and observations as used in this study, remotely sensed satellite data would also provide robust methods of advanced monitoring of ocean acidification.

Acknowledgments

The authors express their gratitude towards the Development of Skilled Manpower in Earth System Sciences (DESK) initiative at the Indian Institute of Tropical Meteorology (IITM), Pune, for facilitating the research work.OTTM model simulations were executed at the ADITYA High-Performance Computing (HPC) of ITM, Pune. SMG sincerely acknowledges the funding support by the Institute of Basic Science (IBS), Republic of Korea, under IBS-R028-D1.

Open Research

Data Availability

Takahashi pH data has been obtained from https://www.ldeo.columbia.edu/res/pi/CO2/carbondioxide/pages/global_ph.html (Takahashi et al., 2014). GFDL reanalysis data has been acquired from https://www.gfdl.noaa.gov/ocean-data-assimilation-model-output/ (Chang et al., 2013) for OTTM model simulations and trend analysis. ROMS model-simulated data presented in this paper are archived at the central data repository of https://incois.gov.in/ and can be obtained by contacting kunal.c@incois.gov.in. All analysis is done using the Pyferret and MATLAB software.

References

Anderson, L. A., & Sarmiento, J. L. (1994). Redfield ratios of remineralization determined by nutrient data analysis. *Global Biogeochemical Cycles*, *8*(1), 65–80. https://doi.org/10.1029/93GB03318

Barker, H. W., Cole, J. N. S., Morcrette, J. J., Pincus, R., Räisänen, P., von Salzen, K., & Vaillancourt, P. A. (2008). The Monte Carlo independent column approximation: An assessment using several global atmospheric models. *Quarterly Journal of the Royal Meteorological Society*, *134*(635). https://doi.org/10.1002/qj.303

Bates, N. R., Best, M. H. P., Neely, K., Garley, R., Dickson, A. G., & Johnson, R. J. (2012). Detecting anthropogenic carbon dioxide uptake and ocean acidification in the North Atlantic Ocean. *Biogeosciences*, *9*(7). https://doi.org/10.5194/bg-9-2509-2012

Bray, N. A., Wijffels, S. E., Chong, J. C., Fieux, M., Hautala, S., Meyers, G., & Morawitz, W. M. L. (1997). Characteristics of the Indo-Pacific throughflow in the eastern Indian Ocean. *Geophysical Research Letters*, *24*(21). https://doi.org/10.1029/97GL51793

Cao, L., Caldeira, K., & Jain, A. K. (2007). Effects of carbon dioxide and climate change on ocean acidification and carbonate mineral saturation. *Geophysical Research Letters*, *34*(5). https://doi.org/10.1029/2006GL028605

Chakraborty, K., Valsala, V., Gupta, G. V. M., & Sarma, V. V. S. S. (2018). Dominant Biological Control Over Upwelling on pCO2 in Sea East of Sri Lanka. *Journal of Geophysical Research: Biogeosciences*, *123*(10). https://doi.org/10.1029/2018JG004446

Chakraborty, K., Valsala, V., Bhattacharya, T., & Ghosh, J. (2021). Seasonal cycle of surface ocean pCO2 and pH in the northern Indian Ocean and their controlling factors. *Progress in Oceanography*, *198*, 102683. https://doi.org/10.1016/J.POCEAN.2021.102683

Chang, Y. S., Zhang, S., Rosati, A., Delworth, T. L., & Stern, W. F. (2013). An assessment of oceanic variability for 1960-2010 from the GFDL ensemble coupled data assimilation. *Climate Dynamics*, *40*(3–4). https://doi.org/10.1007/s00382-012-1412-2

de Deckker, P. (2016). The Indo-Pacific Warm Pool: critical to world oceanography and world climate. *Geoscience Letters*. https://doi.org/10.1186/s40562-016-0054-3

Dommenget, D. (2011). An objective analysis of the observed spatial structure of the tropical Indian Ocean SST variability. *Climate Dynamics*, *36*(11–12). https://doi.org/10.1007/s00382-010-0787-1

Doney, S. C., Fabry, V. J., Feely, R. A., & Kleypas, J. A. (2009). Ocean acidification: The other CO2 problem. *Annual Review of Marine Science*. https://doi.org/10.1146/annurev.marine.010908.163834

Donguy, J. R., & Meyers, G. (1996). Seasonal variations of sea-surface salinity and temperature in the tropical Indian Ocean. *Deep-Sea Research Part I: Oceanographic Research Papers*, *43*(2). https://doi.org/10.1016/0967-0637(96)00009-X

Duarte, C. M., Losada, I. J., Hendriks, I. E., Mazarrasa, I., & Marbà, N. (2013). The role of coastal plant communities for climate change mitigation and adaptation. *Nature Climate Change*. https://doi.org/10.1038/nclimate1970

Egleston, E. S., Sabine, C. L., & Morel, F. M. M. (2010). Revelle revisited: Buffer factors that quantify the response of ocean chemistry to changes in DIC and alkalinity. *Global Biogeochemical Cycles*, *24*(1). https://doi.org/10.1029/2008GB003407

Fairall, C. W., Bradley, E. F., Rogers, D. P., Edson, J. B., & Young, G. S. (1996). Bulk parameterization of air-sea fluxes for Tropical Ocean-Global Atmosphere Coupled-Ocean Atmosphere Response Experiment. *Journal of Geophysical Research: Oceans*, *101*(C2), 3747–3764. https://doi.org/10.1029/95JC03205

Fairall, C. W., Bradley, E. F., Godfrey, J. S., Wick, G. A., Edson, J. B., & Young, G. S. (1996). Cool-skin and warm-layer effects on sea surface temperature. *Journal of Geophysical Research C: Oceans*, *101*(C1). https://doi.org/10.1029/95JC03190

Fassbender, A. J., Sabine, C. L., Feely, R. A., Langdon, C., & Mordy, C. W. (2011). Inorganic carbon dynamics during northern California coastal upwelling. *Continental Shelf Research*, *31*(11). https://doi.org/10.1016/j.csr.2011.04.006

Feely, R. A., Doney, S. C., & Cooley, S. R. (2009). Ocean acidification: Present conditions and future changes in a high-CO 2 world. *Oceanography*, *22*(SPL.ISS. 4). https://doi.org/10.5670/oceanog.2009.95

Fennel, K., Wilkin, J., Levin, J., Moisan, J., O'Reilly, J., & Haidvogel, D. (2006). Nitrogen cycling in the Middle Atlantic Bight: Results from a three-dimensional model and implications for the North Atlantic nitrogen budget. *Global Biogeochemical Cycles*, *20*(3). https://doi.org/10.1029/2005GB002456

Fennel, K., Wilkin, J., Previdi, M., & Najjar, R. (2008). Denitrification effects on air-sea CO2 flux in the coastal ocean: Simulations for the northwest North Atlantic. *Geophysical Research Letters*, *35*(24). https://doi.org/10.1029/2008GL036147

Fine, R. A., Willey, D. A., & Millero, F. J. (2017). Global variability and changes in ocean total alkalinity from Aquarius satellite data. *Geophysical Research Letters*, *44*(1). https://doi.org/10.1002/2016GL071712

Friedlingstein, P., Jones, M. W., O'Sullivan, M., Andrew, R. M., Hauck, J., Peters, G. P., et al. (2019). Global carbon budget 2019. *Earth System Science Data*, *11*(4), 1783–1838. https://doi.org/10.5194/ESSD-11-1783-2019

Gattuso, J. P., Magnan, A., Billé, R., Cheung, W. W. L., Howes, E. L., Joos, F., et al. (2015). Contrasting futures for ocean and society from different anthropogenic CO2 emissions scenarios. *Science*. https://doi.org/10.1126/science.aac4722

Griffies, S. M., & Hallberg, R. W. (2000). Biharmonic friction with a Smagorinsky-like viscosity for use in large-scale eddy-permitting ocean models. *Monthly Weather Review*, *128*(8 II). https://doi.org/10.1175/1520-0493(2000)128<2935:bfwasl>2.0.co;2

Guinotte, J. M., & Fabry, V. J. (2008). Ocean Acidification and Its Potential Effects on Marine Ecosystems. *Annals of the New York Academy of Sciences*, *1134*(1), 320–342. https://doi.org/10.1196/ANNALS.1439.013

Hagens, M., & Middelburg, J. J. (2016). Attributing seasonal pH variability in surface ocean waters to governing factors. *Geophysical Research Letters*, *43*(24). https://doi.org/10.1002/2016GL071719

H.-O. Pörtner, D.C. Roberts, M. Tignor, E.S. Poloczanska, K. Mintenbeck, A. Alegría, et al. (2022). IPCC, 2022: Climate Change 2022: Impacts, Adaptation and Vulnerability | Climate Change 2022: Impacts, Adaptation and Vulnerability. Retrieved March 24, 2022, from https://www.ipcc.ch/report/ar6/wg2/

Hönisch, B., Ridgwell, A., Schmidt, D. N., Thomas, E., Gibbs, S. J., Sluijs, A., et al. (2012). The geological record of ocean acidification. *Science*, *335*(6072), 1058–1063. https://doi.org/10.1126/SCIENCE.1208277/SUPPL_FILE/HOENISCH_CARBONATE_CHEM_TUTORIAL.PDF

Horii, T., Ueki, I., Ando, K., Hasegawa, T., Mizuno, K., & Seiki, A. (2016). Impact of intraseasonal salinity variations on sea surface temperature in the eastern equatorial Indian Ocean. *Journal of Oceanography*, *72*(2). https://doi.org/10.1007/s10872-015-0337-x

Kapsenberg, L., Alliouane, S., Gazeau, F., Mousseau, L., & Gattuso, J. P. (2017). Coastal ocean acidification and increasing total alkalinity in the northwestern Mediterranean Sea. *Ocean Science*, *13*(3), 411–426. https://doi.org/10.5194/OS-13-411-2017

Key, R. M., Kozyr, A., Sabine, C. L., Lee, K., Wanninkhof, R., Bullister, J. L., et al. (2004). A global ocean carbon climatology: Results from Global Data Analysis Project (GLODAP). *Global Biogeochemical Cycles*, *18*(4), 1–23. https://doi.org/10.1029/2004GB002247

Landschützer, P., Gruber, N., & Bakker, D. C. E. (2016). Decadal variations and trends of the global ocean carbon sink. *Global Biogeochemical Cycles*, *30*(10), 1396–1417. https://doi.org/10.1002/2015GB005359

Large, W. G., McWilliams, J. C., & Doney, S. C. (1994). Oceanic vertical mixing: A review and a model with a nonlocal boundary layer parameterization. *Reviews of Geophysics*, *32*(4), 363–403. https://doi.org/10.1029/94RG01872

Laurent, A., Fennel, K., Cai, W. J., Huang, W. J., Barbero, L., & Wanninkhof, R. (2017). Eutrophication-induced acidification of coastal waters in the northern Gulf of Mexico: Insights into origin and processes from a coupled physical-biogeochemical model. *Geophysical Research Letters*, *44*(2). https://doi.org/10.1002/2016GL071881

Li, J., & Barker, H. W. (2005). A radiation algorithm with correlated-k distribution. Part I: Local thermal equilibrium. *Journal of the Atmospheric Sciences*, *62*(2). https://doi.org/10.1175/JAS-3396.1

Liu, W. T., Katsaros, K. B., & Businger, J. A. (1979). Bulk parameterization of air-sea exchanges of heat and water vapor including the molecular constraints at the interface. *Journal of Atmospheric Sciences*, *36*(9). https://doi.org/10.1175/1520-0469(1979)036<1722:BPOASE>2.0.CO;2

Luchetta, A., Cantoni, C., & Catalano, G. (2010). New observations of CO2-induced acidification in the northern Adriatic Sea over the last quarter century. *Chemistry and Ecology*, *26*(SUPPL. 1). https://doi.org/10.1080/02757541003627688

Midorikawa, T., Ishii, M., Saito, S., Sasano, D., Kosugi, N., Motoi, T., et al. (2010). Decreasing pH trend estimated from 25-yr time series of carbonate parameters in the western North Pacific. *Tellus, Series B: Chemical and Physical Meteorology*, *62*(5). https://doi.org/10.1111/j.1600-0889.2010.00474.x

Midorikawa, T., Inoue, H. Y., Ishii, M., Sasano, D., Kosugi, N., Hashida, G., et al. (2012). Decreasing pH trend estimated from 35-year time series of carbonate parameters in the Pacific sector of the Southern Ocean in

summer. *Deep-Sea Research Part I: Oceanographic Research Papers*, *61*. https://doi.org/10.1016/j.dsr.2011.12.003

Najjar, R., & Orr, J. (1998). Design of OCMIP-2 simulations of chlorofluorocarbons, the solubility pump and common biogeochemistry. *Internal OCMIP Report*, *25*. Retrieved from Retrieved from http://ocmip5.ipsl.fr/documentation/OCMIP/phase2/simulations/design.ps

Peters, W., Jacobson, A. R., Sweeney, C., Andrews, A. E., Conway, T. J., Masarie, K., et al. (2007). An atmospheric perspective on North American carbon dioxide exchange: CarbonTracker. *Proceedings of the National Academy of Sciences of the United States of America*, *104*(48). https://doi.org/10.1073/pnas.0708986104

Petit, J. R., Jouzel, J., Raynaud, D., Barkov, N. I., Barnola, J. M., Basile, I., et al. (1999). Climate and atmospheric history of the past 420,000 years from the Vostok ice core, Antarctica. *Nature 1999 399:6735*, *399*(6735), 429–436. https://doi.org/10.1038/20859

le Quéré, C., Andrew, R. M., Friedlingstein, P., Sitch, S., Pongratz, J., Manning, A. C., et al. (2018). Global Carbon Budget 2017. *Earth System Science Data*, *10*(1). https://doi.org/10.5194/essd-10-405-2018

Rao, D. N., & Sarma, V. V. S. S. (2022). Accumulation of dissolved organic carbon and nitrogen in the photic zone in the nitrogen-depleted waters of the Bay of Bengal. *Marine Chemistry*, *239*, 104074. https://doi.org/10.1016/J.MARCHEM.2021.104074

Redi, M. H. (1982). Oceanic isopycnal mixing by coordinate rotation. *Journal of Physical Oceanography*, *12*(10). https://doi.org/10.1175/1520-0485(1982)012<1154:OIMBCR>2.0.CO;2

Rhein, M. , Rintoul, S. R. , Aoki, S. , Campos, E. , Chambers, D. , Feely, R. A. , et al. (2013). Observations: Ocean. In: Climate Change 2013: The Physical Science Basis. Contribution of Working Group I to the Fifth Assessment Report of the Intergovernmental Panel on Climate Change. Retrieved March 24, 2022, from https://www.researchgate.net/publication/284806346_Observations_Ocean_In_Climate_Change_2013_The_Physical_Science_Basis_Contribution_of_Working_Group_I_to_the_Fifth_Assessment_Report_of_the_Intergovernmental_Panel_on_Climate_Change

Sabine, C. L., Key, R. M., Feely, R. A., & Greeley, D. (2002). Inorganic carbon in the Indian Ocean: Distribution and dissolution processes. *Global Biogeochemical Cycles*, *16*(4). https://doi.org/10.1029/2002gb001869

Sabine, C. L., Feely, R. A., Gruber, N., Key, R. M., Lee, K., Bullister, J. L., et al. (2004). The oceanic sink for anthropogenic CO2. *Science*, *305*(5682). https://doi.org/10.1126/science.1097403

von Salzen, K., McFarlane, N. A., & Lazare, M. (2005). The role of shallow convection in the water and energy cycles of the atmosphere. *Climate Dynamics*, *25*(7–8). https://doi.org/10.1007/s00382-005-0051-2

Sarma, V. V. S. S., Lenton, A., Law, R. M., Metzl, N., Patra, P. K., Doney, S., et al. (2013). Sea-air CO 2 fluxes in the Indian Ocean between 1990 and 2009. *Biogeosciences*, *10*, 7035–7052. https://doi.org/10.5194/bg-10-7035-2013

Sarmiento, J. L., & Gruber, N. (2006). *Ocean Biogeochemical Dynamics*. *OCEAN BIOGEOCHEMICAL DYNAMICS*. Princeton University Press. Retrieved from http://press.princeton.edu/titles/8223.html

Schott, F. A., & McCreary, J. P. (2001). The monsoon circulation of the Indian Ocean. *Progress in Oceanography*. https://doi.org/10.1016/S0079-6611(01)00083-0

Sharada, M. K., Swathi, P. S., Yajnik, K. S., & Devasena, C. K. (2008). Role of biology in the air-sea carbon flux in the Bay of Bengal and Arabian Sea. *Journal of Earth System Science*, *117*(4). https://doi.org/10.1007/s12040-008-0043-9

Sreeush, M. G., Valsala, V., Pentakota, S., Prasad, K. V. S. R., & Murtugudde, R. (2018). Biological production in the Indian Ocean upwelling zones - Part 1: Refined estimation via the use of a variable compensation depth in ocean carbon models. *Biogeosciences*, *15*(7), 1895–1918. https://doi.org/10.5194/BG-15-1895-2018

Sreeush, M. G., Rajendran, S., Valsala, V., Pentakota, S., Prasad, K. V. S. R., & Murtugudde, R. (2019). Variability, trend and controlling factors of Ocean acidification over Western Arabian Sea upwelling region. *Marine Chemistry*, *209*. https://doi.org/10.1016/j.marchem.2018.12.002

Sreeush, M. G., Valsala, V., Santanu, H., Pentakota, S., Prasad, K. V. S. R., Naidu, C. v., & Murtugudde, R. (2020). Biological production in the Indian Ocean upwelling zones - Part 2: Data based estimates of variable compensation depth for ocean carbon models via cyclo-stationary Bayesian Inversion. *Deep-Sea Research Part II: Topical Studies in Oceanography*, *179*. https://doi.org/10.1016/j.dsr2.2019.07.007

Susanto, R. D., Gordon, A. L., & Zheng, Q. (2001). Upwelling along the coasts of Java and Sumatra and its relation to ENSO. *Geophysical Research Letters*, *28*(8). https://doi.org/10.1029/2000GL011844

Takahashi, T., Sutherland, S. C., Wanninkhof, R., Sweeney, C., Feely, R. A., Chipman, D. W., et al. (2009). Climatological mean and decadal change in surface ocean pCO2, and net sea-air CO2 flux over the global oceans. *Deep-Sea Research Part II: Topical Studies in Oceanography*, *56*(8–10). https://doi.org/10.1016/j.dsr2.2008.12.009

712 Takahashi, T., Sutherland, S. C., Chipman, D. W., Goddard, J. G., & Ho, C. (2014). Climatological distributions of
713 pH, pCO2, total CO2, alkalinity, and CaCO3 saturation in the global surface ocean, and temporal changes at
714 selected locations. *Marine Chemistry*, *164*. https://doi.org/10.1016/j.marchem.2014.06.004
715 Tarique, M., Rahaman, W., Fousiya, A. A., Lathika, N., Thamban, M., Achyuthan, H., & Misra, S. (2021). Surface
716 pH Record (1990–2013) of the Arabian Sea From Boron Isotopes of Lakshadweep Corals—Trend,
717 Variability, and Control. *Journal of Geophysical Research: Biogeosciences*, *126*(7), e2020JG006122.
718 https://doi.org/10.1029/2020JG006122
719 Valsala, V, & Maksyutov, S. (2010). Simulation and assimilation of global ocean pCO2 and air–sea CO2 fluxes
720 using ship observations of surface ocean pCO2 in a simplified biogeochemical offline model. *Tellus B:*
721 *Chemical and Physical Meteorology*, *62*(5), 821–840. https://doi.org/10.1111/J.1600-0889.2010.00495.X
722 Valsala, V. , & Maksyutov, S. (2013). Interannual variability of the air-sea CO2 flux in the north Indian Ocean Vinu
723 Valsala. *Ocean Dynamics*, *63*, 165–178. https://doi.org/10.1007/s10236-012-0588-7
724 Valsala, Vinu, & Murtugudde, R. (2015). Mesoscale and intraseasonal air–sea CO2 exchanges in the western
725 Arabian Sea during boreal summer. *Deep Sea Research Part I: Oceanographic Research Papers*, *103*, 101–
726 113. https://doi.org/10.1016/J.DSR.2015.06.001
727 Valsala, Vinu, Maksyutov, S., & Motoyoshi, I. (2008). Design and validation of an offline oceanic tracer transport
728 model for a carbon cycle study. *Journal of Climate*, *21*(12). https://doi.org/10.1175/2007JCLI2018.1
729 Valsala, Vinu, Maksyutov, S., & Murtugudde, R. (2012). A window for carbon uptake in the southern subtropical
730 Indian Ocean. *Geophysical Research Letters*, *39*(17). https://doi.org/10.1029/2012GL052857
731 Valsala, Vinu, Sreeush, M. G., & Chakraborty, K. (2020). The IOD Impacts on the Indian Ocean Carbon Cycle.
732 *Journal of Geophysical Research: Oceans*, *125*(11). https://doi.org/10.1029/2020JC016485
733 Wanninkhof, R., Park, G. H., Takahashi, T., Sweeney, C., Feely, R., Nojiri, Y., et al. (2013). Global ocean carbon
734 uptake: Magnitude, variability and trends. *Biogeosciences*, *10*(3). https://doi.org/10.5194/bg-10-1983-2013
735 Wanninkhof, Rik. (2014). Relationship between wind speed and gas exchange over the ocean revisited. *Limnology*
736 *and Oceanography: Methods*, *12*(JUN). https://doi.org/10.4319/lom.2014.12.351
737 Waters, J. F., Millero, F. J., & Sabine, C. L. (2011). Changes in South Pacific anthropogenic carbon. *Global*
738 *Biogeochemical Cycles*, *25*(4). https://doi.org/10.1029/2010GB003988
739 Xue, L., Yu, W., Wang, H., Jiang, L. Q., Feng, L., Gao, L., et al. (2014). Temporal changes in surface partial
740 pressure of carbon dioxide and carbonate saturation state in the eastern equatorial Indian Ocean during the
741 1962–2012 period. *Biogeosciences*. https://doi.org/10.5194/bg-11-6293-2014
742 Zahariev, K., Christian, J. R., & Denman, K. L. (2008). Preindustrial, historical, and fertilization simulations using a
743 global ocean carbon model with new parameterizations of iron limitation, calcification, and N2 fixation.
744 *Progress in Oceanography*, *77*(1). https://doi.org/10.1016/j.pocean.2008.01.007
745 Zeebe, R. E. (2012). History of Seawater Carbonate Chemistry, Atmospheric CO2, and Ocean Acidification.
746 *Http://Dx.Doi.Org/10.1146/Annurev-Earth-042711-105521*, *40*, 141–165.
747 https://doi.org/10.1146/ANNUREV-EARTH-042711-105521
748 Zeebe, R. E., & Wolf-Gladrow, D. A. (2001). *CO2 in seawater : equilibrium, kinetics, isotopes*. Elsevier
749 Oceanography Series. Retrieved from https://www.elsevier.com/books/co2-in-seawater-equilibrium-kinetics-
750 isotopes/zeebe/978-0-444-50946-8
751